A.S. Vivekananda*, S. Balasivanandha Prabu and R. Paskaramoorthy

Processing-structure-property correlations of *in situ* Al/TiB_2 composites processed by aluminothermic reduction process

DOI 10.1515/secm-2017-0014
Received January 12, 2017; accepted June 2, 2017; previously published online July 22, 2017

Abstract: This paper reports the influence of process parameters on the size and distribution of *in situ* titanium diboride (TiB_2) particles within the aluminium (Al) matrix. TiB_2 particles were formed as a result of the *in situ* reaction of potassium hexafluorotitanate (K_2TiF_6) and potassium tetra fluoroborate (KBF_4) with molten Al. Two process parameters, namely, the addition time (AT) and holding time (HT) of precursor salts, were considered. The Al/TiB_2 composites were produced by allowing the *in situ* reaction to occur at various ATs (10, 20, and 30 min) and HTs (20, 30, and 40 min). Results showed that the formation of TiB_2 was confirmed by XRD analysis. The microstructure, TiB_2 particle size, hardness, yield strength (YS), and ultimate tensile strength (UTS) were strongly affected by the said process parameters. The variations in hardness and UTS were highly consistent with those found in the microstructure of the composites. Compared with the Al parent material, the increase in the average hardness and UTS of the composite were 51% and 44%, respectively. This improvement was achieved for the composite sample fabricated with 20 min of AT and 30 min of HT. At this condition, the composite displayed near-uniform particle distribution.

Keywords: *in situ* reaction; mechanical properties; metal matrix composites; microstructures.

1 Introduction

Particle-reinforced metal matrix composites (PRMMCs) are used in the aerospace, automobile, electronic packaging, and transportation industries due to their superior mechanical and thermal properties, such as high strength to weight ratio, high thermal stability, chemical stability, and good wear resistance [1, 2]. Different conventional processing techniques, such as solid-state [3], liquid-state [4], and vapor-state processing [5], are available for making PRMMCs. Among these, the liquid-state processing route has been mostly used because it can produce complex-shaped components in an efficient manner.

PRMMCs can be fabricated via both the *ex situ* and *in situ* processing routes. The *in situ* processing routes are often favored for making PRMMCs, as these routes overcome the technical challenges encountered in the *ex situ* processing routes. The technical challenges include non-uniform distribution of particles, interphase formation, and non-wetting of reinforcement with the matrix [4, 6]. A number of *in situ* reactions methods, such as solid–solid [7], solid–liquid [8], liquid–liquid [9], and vapor–liquid–solid [10] reaction methods have been developed. Among these, the solid–liquid reaction method has become one of the most commonly used techniques for the processing of Al/TiB_2 composites.

In recent times, titanium diboride (TiB_2)-reinforced metal matrix composites have gained attention for wear-resistance applications as they have high wear resistance, low co-efficient of thermal expansion, high thermal stability, and high thermal conductivity [1, 2, 11]. A number of studies have been carried out for understanding the growth and distribution of TiB_2 within the matrix, because of the size, distribution, and quantity of particles that have significant influences on the mechanical properties of composites.

Xue et al. [12] fabricated Al-5vol.%TiB_2 composites using the flux-assisted synthesis route. They reported an improvement in the dispersion of TiB_2 particles in the aluminum melt due to the addition of CeO_2 during the process. Watson et al. [13] synthesized Al/TiB_2 composites using *in situ* reaction and reported improved distribution of TiB_2 particles within the matrix upon increasing the holding time (HT). Chen et al. [14] fabricated Al/TiB_2 composites using TiO_2, H_3BO_3, and Na_3AlF_6, and reported uniform dispersion of particles in the matrix. Mallikarjuna et al. [15] observed a decrease in the grain size of the aluminum

***Corresponding author: A.S. Vivekananda,** Department of Mechanical Engineering, College of Engineering Guindy, Anna University, Chennai-600025, India, Tel.: +91-44-22357760, Fax: +91-44-22357744, e-mail: lance.vivek@gmail.com
S. Balasivanandha Prabu: Department of Mechanical Engineering, College of Engineering Guindy, Anna University, Chennai, India
R. Paskaramoorthy: DST/NRF Centre for Strong Materials and School of Mechanical, Industrial and Aeronautical Engineering, University of the Witwatersrand, Johannesburg, South Africa

matrix in the Al/TiB_2 system when the HT was increased. The formation of TiB_2 facilitates grain refinement in the matrix material has also been reported. Emamy et al. [16] explained the formation mechanism of *in situ* TiB_2 particles in an Al matrix material, and reported that diffusion of boron particle into Al_3Ti to form TiB_2 particles improved at higher HT and temperature. This favorable condition also helps in the dissolution of Al_3Ti. All these work reported the promotion of uniform particle distribution achieved at sufficiently high HT due to the sufficient time for redistribution.

Murty et al. [17] fabricated an Al-5Ti-B master alloy through halide–salt reaction, and investigated the effects of various parameters, such as the sequence of addition of salts, reaction time, influence of stirring, presence of impurities (Cr, Zr and Si), and addition of Mg, on the grain refinement. Liu et al. [18] reported the improved dispersion of TiB_2 via ultrasonically assisted salt–metal reaction. The formation of TiB_2 also increased in ultrasonically assisted salt–melt reaction when compared to mechanical stirring.

Lu et al. [19] have synthesized TiB_2 via exothermic reaction by using K_2TiF_6 and KBF_4 salts. They also investigated the size of TiB_2 particles, grain refinement, and strength of composite with respect to the HT. They reported reaction being slow when salts were added at a slower rate into the Al melt, but that the reaction was completed at a higher HT. These results help in understanding the influence of the AT of salts and HT on the reaction between salts and size of TiB_2 particles and the properties of the composites.

Gao et al. [20] fabricated Al-Cu/5vol.%TiB_2 through *in situ* reaction using the halide–salt route. The successful fabrication of the composite with a uniform distribution of TiB_2 particle resulted in improved mechanical properties. They also reported that the precipitate of the Al-Cu alloy, known as Al_2Cu, wet the TiB_2 into the Al melt.

Chen et al. [21] fabricated Al-5 wt%TiB_2 composite through the flux-assisted synthesis using K_2TiF_6 and KBF_4 salts with different process parameters, such as HT, holding temperature, stirring time, and stirring speed. They also reported higher Ti and B recovery at higher HT.

The literature has shown that particle formation and its distribution are influenced by several parameters, including melt temperature, AT, and HT. While the previously mentioned works have considered the effect of HT, the combined effects of the AT and HT of precursor salts have not been investigated. Accordingly, this paper discusses the microstructure and the mechanical properties of the Al/TiB_2 composites processed at different ATs and HTs.

2 Materials and methods

Aluminum (A380) alloy was used as the matrix material. The chemical composition of the matrix material is given in Table 1. It has good castability characteristics, such as fluidity and the absence of hot tearing due to higher amount of silicon. The details of processing parameters are given in Table 2. A weighted quantity of matrix material was melted in a graphite crucible, and the temperature of the melt was maintained at 700°C by using an electrical resistant furnace. The same temperature of the melt was used in all different combinations of processing parameters.

The halide salts K_2TiF_6 and KBF_4 were used as precursors to form *in situ* TiB_2. To form 5wt.%TiB_2 in the melt, the quantities of the salts were determined based on stoichiometric calculations [2]. The precursors were added to the melt at different rates, as indicated in Table 2. Sodium cryolite was added to the melt after adding the precursors. This was done to suppress the Al_2O_3 formation within the melt and to accelerate the reaction by reducing surface energy [22].

The TiB_2 particles were formed through the dissolution precipitation mechanism. The sequence of the reaction between Al alloy and precursors are given below [20].

$$3K_2TiF_6 + 13Al \rightarrow 3Al_3Ti + 3KAlF_4 + K_3AlF_6 \quad (1)$$

$$2KBF_4 + 3Al \rightarrow AlB_2 + 2KAlF_4 \quad (2)$$

$$Al_3Ti + AlB_2 \rightarrow TiB_2 + 4Al \quad (3)$$

The KBF_4 salt should be added first into the melt due to the low recovery rate of B and also to prevent the emulsification and oxidation of K_2TiF_6. The KBF_4 and K_2TiF_6 were reacted with Al to form Al_3Ti and AlB_2, and the reaction

Table 1: Composition of the aluminum (A380) alloy.

Elements	Cu	Mg	Si	Fe	Mn	Ni	Zn	Pb	Sn	Ti	Al
%wt	3.22	0.19	8.72	0.98	0.38	0.04	1.47	0.15	0.02	0.03	84.8

Table 2: Processing conditions for the fabrication of composites.

Melt temperature (°C)	AT of precursors (min)	HT (min)
700	10, 20, 30	20
	10, 20, 30	30
	10, 20, 30	40

was continued until Ti and B reached saturation in the melt. Further, the small atomic size of boron diffused into Al_3Ti and formed TiB_2 particles [16]. This reaction continued until B presented in the melt. The dense quantity of TiB_2 formation led to agglomeration, which was avoided by mechanical stirring. A mild-steel stirrer coated with zirconia was used for mechanically stirring of the melt [15]. The speed of the impeller was kept at 400 rpm. The duration of stirring was the same as the HT. After stirring, the slag floating on top of the melt was removed. Finally, the composite was cast by pouring the slurry into a steel die pre-heated to 300°C. The fabrication was carried out in a protective atmosphere using argon gas in order to prevent the contamination of melt by oxygen.

The cast specimens were characterized for particle distribution and mechanical properties. Two samples were fabricated for each processing condition. Samples from the top, middle, and bottom of the cast were cut for the microstructure analysis, which was carried out using an optical microscope (Metavis Model MM 25 IS, Japan) and a scanning electron microscope (SEM, Hitachi S3400N, Japan). Hardness distribution was measured using a Brinell hardness tester according to the ASTM-E10 standard. The tensile strength was measured using a INSTRON machine according to the ASTM-B557M standard. The XRD analysis was carried out using an X-ray diffractometer (PANalytical X'Pert-PRO XRD, USA; step size-0.02, wavelength of Cu-Kα-1.54 angstrom) to confirm the formation of TiB_2 particles. The TiB_2 particles were extracted by immersing the composite specimens in a chemical solution bath of NaOH and distilled water. The size distribution of extracted particles was determined by using a nanoanalyzer [Dynamic light scattering (DLS), Malvern Zetasizer ver.7.1, UK] which was working under light scattering technique. The cumulant analysis yielded the mean particle size of the sample from the received data. The morphology of extracted particles was studied by using a transmission electron microscope (Hitachi, H7650, Japan).

3 Results and discussion

3.1 Microstructure analysis

Figure 1A and B present the microstructure of the parent Al (A380) alloy and Al/TiB_2 composite, respectively. The microstructure of the Al (A380) alloy contained silicon (Si) needles, which were segregated to the grain boundaries. No dendrite grain structure was found in the composite samples due to TiB_2 formation (Figure 1B) and the particles dispersed with Si along the grain boundaries of Al Alloy. TiB_2 particles restricted dendrite growth by nucleating to a large number of α-Al grains. The uniform dispersion of particles and the restriction of dendrites were the main factors that improved the strength of the composite. The dispersion of particles is explained in the following section.

Figures 2 to 4 show the microstructures of samples fabricated with different ATs and HTs. Figure 2A–C show the microstructure of the samples fabricated at 10 min AT and various HTs of 20, 30, and 40 min, respectively. Varying degrees of particle agglomeration could be seen

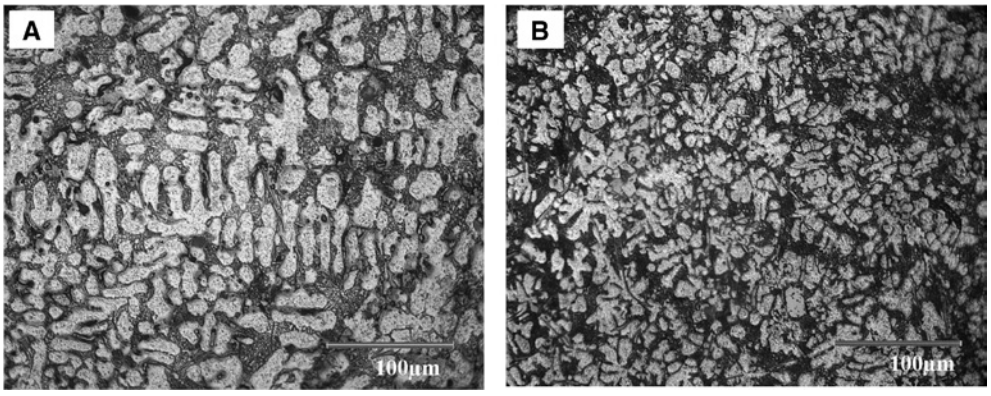

Figure 1: Microstructures of the (A) Al (A380) alloy and (B) Al/TiB_2 composite processed at 10 min AT and 20 min HT.

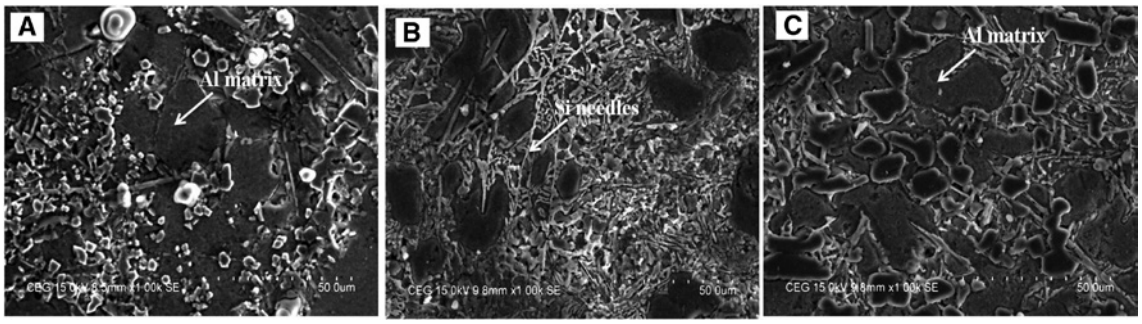

Figure 2: Microstructures of the Al/TiB_2 composites fabricated at 10 min AT and HTs of (A) 20 min (B) 30 min, and (C) 40 min.

in the figures. Figure 2A shows, perhaps, the worst case of particle agglomeration. The reaction rate of precursors with the Al melt was fast for a short AT. As a result, particles were formed within a short time and the resulting particle sizes tended to be large. Moreover, the incomplete reaction may have been due to short ATs and HTs. Due to their weight, the size of the particles resisted stirring and settled quickly to the bottom of the melt, thus resulting in agglomeration. However, the degree of agglomeration remained the same even if the HT increased, as shown in Figure 2B and C.

Figures 3 and 4 show the microstructures of the samples fabricated with various HTs and ATs of 20 and 30 min, respectively. As can be seen, particle dispersion was better in Figure 3A–C than in the samples processed at the shorter AT of 10 min, shown in Figure 2A–C. In particular, the microstructures shown in Figure 3B and C, which correspond to 20 min of AT and 30 and 40 min of HT, respectively, displayed the least particle agglomeration. Figure 4A–C, corresponding to 30 min of AT and 20, 30, and 40 min of HT, respectively, display the worst agglomeration of particles.

In general, good particle distributions were observed in the composites processed at 30 min HT as there was sufficient reaction time to induce the formation of TiB_2 particles and their distribution (Figure 3B). Figure 3C also

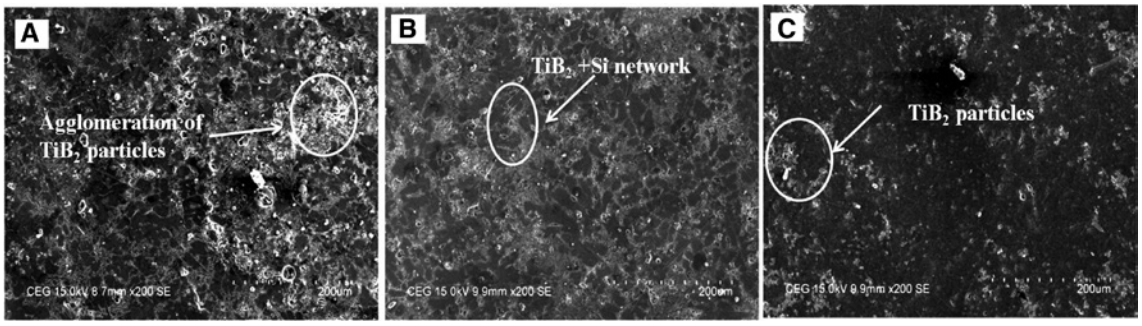

Figure 3: Microstructures of the Al/TiB_2 composites fabricated at 20 min AT and HTs of (A) 20 min (B) 30 min, and (C) 40 min.

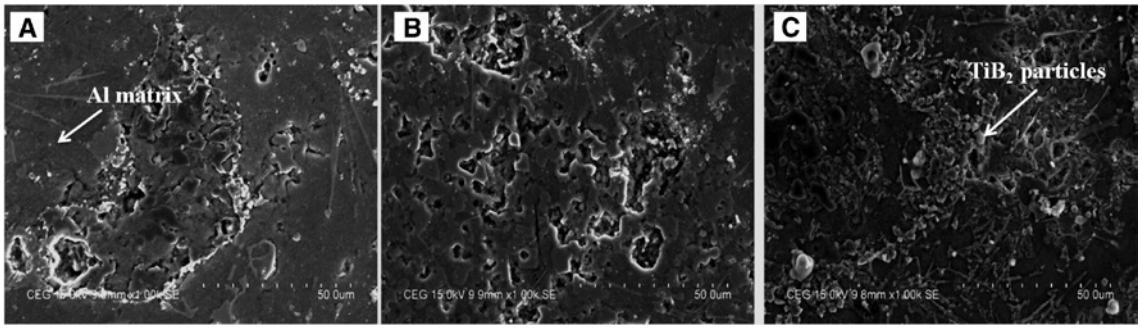

Figure 4: Microstructures of the Al/TiB_2 composite fabricated at 30 min AT and HTs of (A) 20 min, (B) 30 min, and (C) 40 min.

shows a fairly good distribution of particles. However, composites processed at 40 min HT (Figure 2C and 4C) display poor distribution of particles. This could be due to two reasons. First, the shorter AT of precursors into the Al melt initially caused faster reaction rate, resulting in a large-sized particle. Second, during the holding period, the particles moved along circular paths due to stirring and experienced centrifugal force; as a result, they moved out and eventually promoted particle agglomeration. Consequently, a long HT could result in significant particle agglomeration.

Figure 5 shows the variation in the clustering index with the AT of precursors for different HTs. The clustering index is defined as the ratio of the number of sub-domains within the cluster and total number of sub-domains. This is an alternative way of presenting the microstructural homogeneity. To calculate the clustering index for each of the conditions, the microstructure was segmented into square arrays of equal dimension with known dimension. The total number of domains with cluster was counted for calculating clustering index. The clusters are defined as the 5% concentration of particles in a particular domain. Figure 5 shows the near-zero clustering index for the composite processed with 20 min AT and 30 min HT. On the one hand, the corresponding microstructure (Figure 3B) shows the best particle distribution. On the other hand, the composite processed with 10 min AT and 20 min HT shows the highest clustering index. The corresponding microstructure (Figure 2A) shows significant particle agglomeration.

From the above discussions, we can say that the particles were well dispersed in a composite processed with 20 min AT 30 min HT condition due to sufficient reaction time that induced particle distribution. At lower AT, i.e. 10 min, the particles were agglomerated heavily irrespective of the HT. This is due to the instantaneous reaction occurring between the precursors, which produced coarser particle sizes.

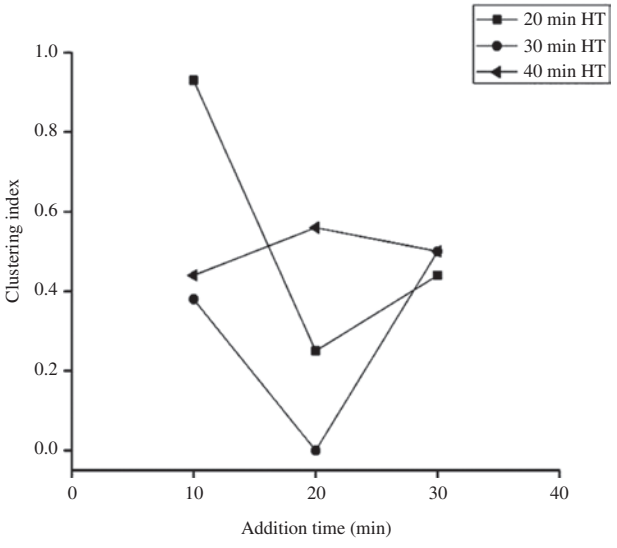

Figure 5: Variation of clustering index with respect to constant AT.

3.2 XRD analysis

The results of XRD analysis for the composite specimen processed with different HTs are shown in Figure 6. The various peaks in the XRD patterns confirm the formation of TiB_2; these peaks also proved that the formation of TiB_2 particles increased when HT increased. The absence of Al_3Ti and AlB_2 is shown in all these conditions.

3.3 Shape and distribution of particle size

The size of the particles formed during the *in situ* reaction is one of the major influencing factors affecting the strength and hardness of composites. The rate of plastic deformation is also controlled by the size of the particle. Figure 7 shows the morphology of the extracted TiB_2 particles, the shape of which is hexagonal.

Figures 8–10 show the variations in the size of the extracted TiB_2 particles for various addition and HTs. Details of the average particle size are given in Table 3. Some trends in the particle size can be seen. For any

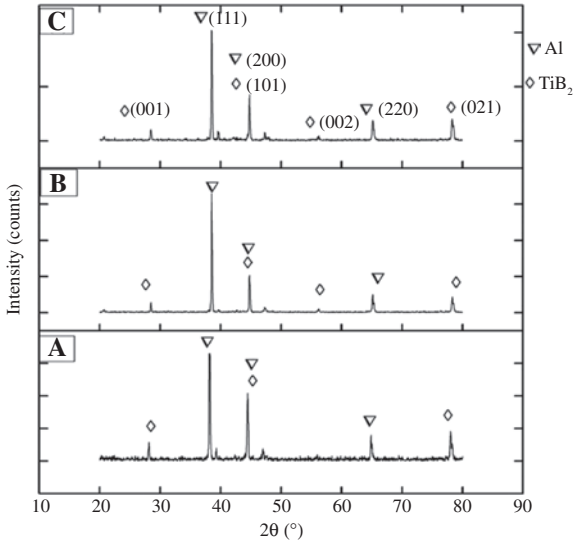

Figure 6: X-Ray diffraction patterns for *in situ* Al/TiB_2 composites processed at 20 min AT and HTs of (A) 20 min, (B) 30 min, and (C) 40 min.

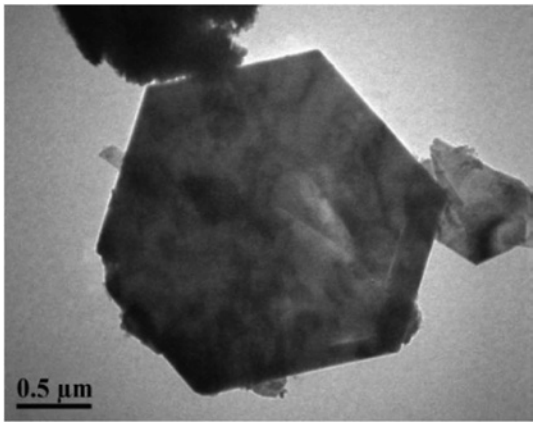

Figure 7: Morphology of the extracted TiB_2 particle.

given AT, the particle size decreased with increase in the HT. An exception to this observation was the composite processed with 30 min AT and 40 min HT; this composite contained the largest particle size. The reason for this anomaly is unclear at present. With regards AT, it is more difficult to observe a trend. For instance, the particle size of the composites processed at 20 min HT initially increased when the AT increased from 10 min to 20 min. A further increase in AT to 30 min saw an increase in particle size. In contrast, the composites processed at both 30 and 40 min HTs displayed just the opposite trend, i.e. initial decrease and subsequent increase with the AT. In view of these observations, one can conclude that combining ATs and HTs is more important than either the AT or HT alone. Moreover, finer particles formed at 20 min AT with 30 and 40 min HT conditions due to the gradual reaction between precursors than in other processing conditions.

3.4 Hardness measurements

Hardness was measured using a Brinell hardness tester according to the ASTM E10 standard. Hardness measurements were taken at nine different locations along the length of the specimen at 20-mm intervals. Figure 11 shows the variations in hardness for different ATs and HTs. As can be seen, all composites showed higher hardness than the parent Al alloy. This can be attributed to the presence of TiB_2 particles that are harder than Al. A small degree of anomaly was observed for the specimen fabricated with 10 min AT and 20 min HT (Figure 11A). The hardness value of this composite measured at the 180-mm location was the same as that of the Al alloy. The absence of TiB_2 at the edge

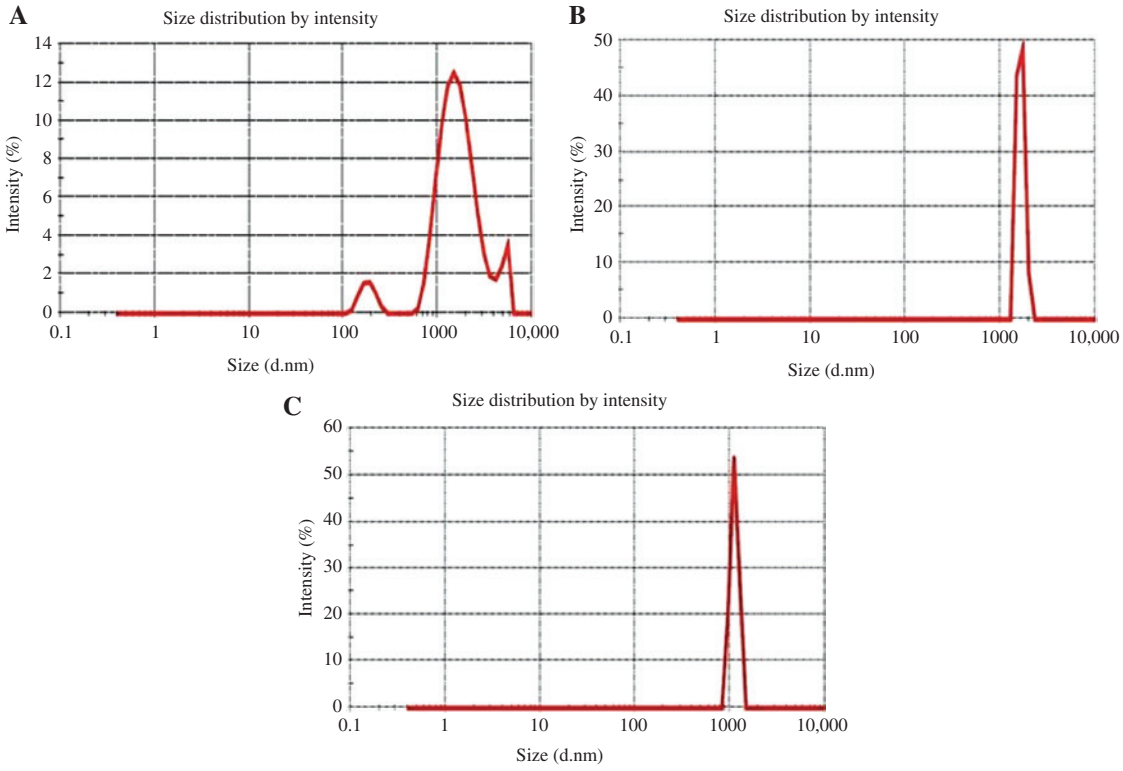

Figure 8: Size distributions of particles for A380 alloy/TiB_2 composites fabricated at 10 min AT and HTs of (A) 20 min, (B) 30 min, and (C) 40 min.

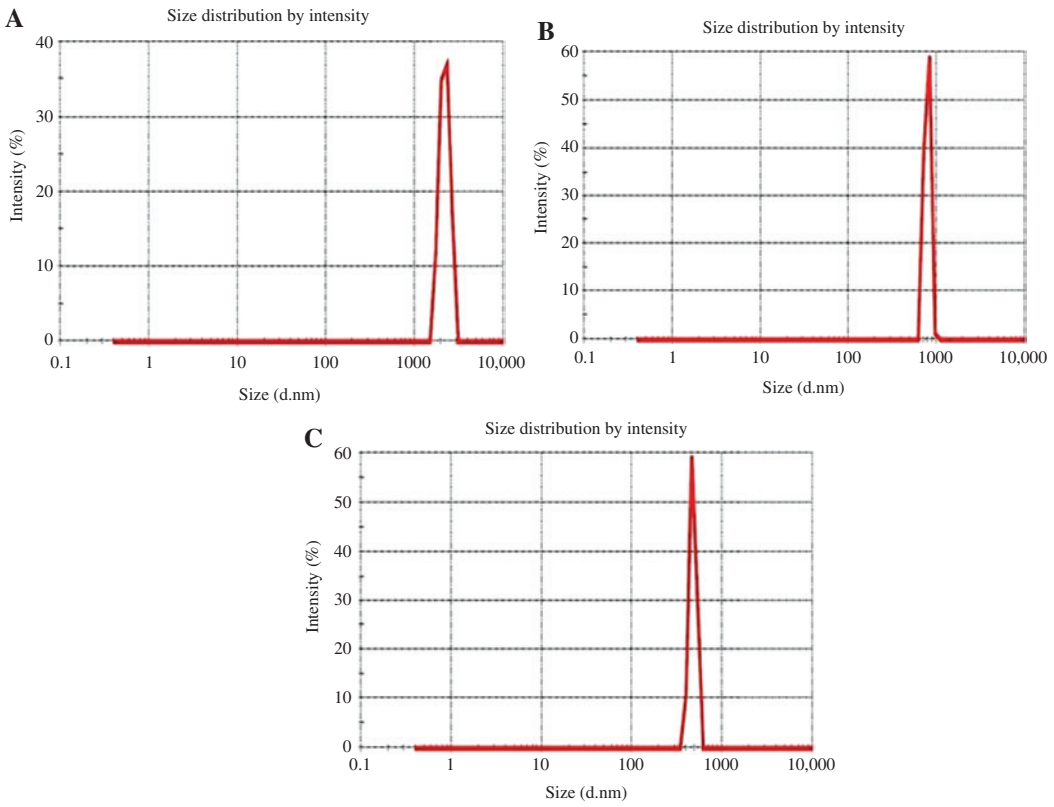

Figure 9: Size distributions of particles for A380 alloy/TiB_2 composites fabricated at 20 min AT and HTs of (A) 20 min, (B) 30 min, and (C) 40 min.

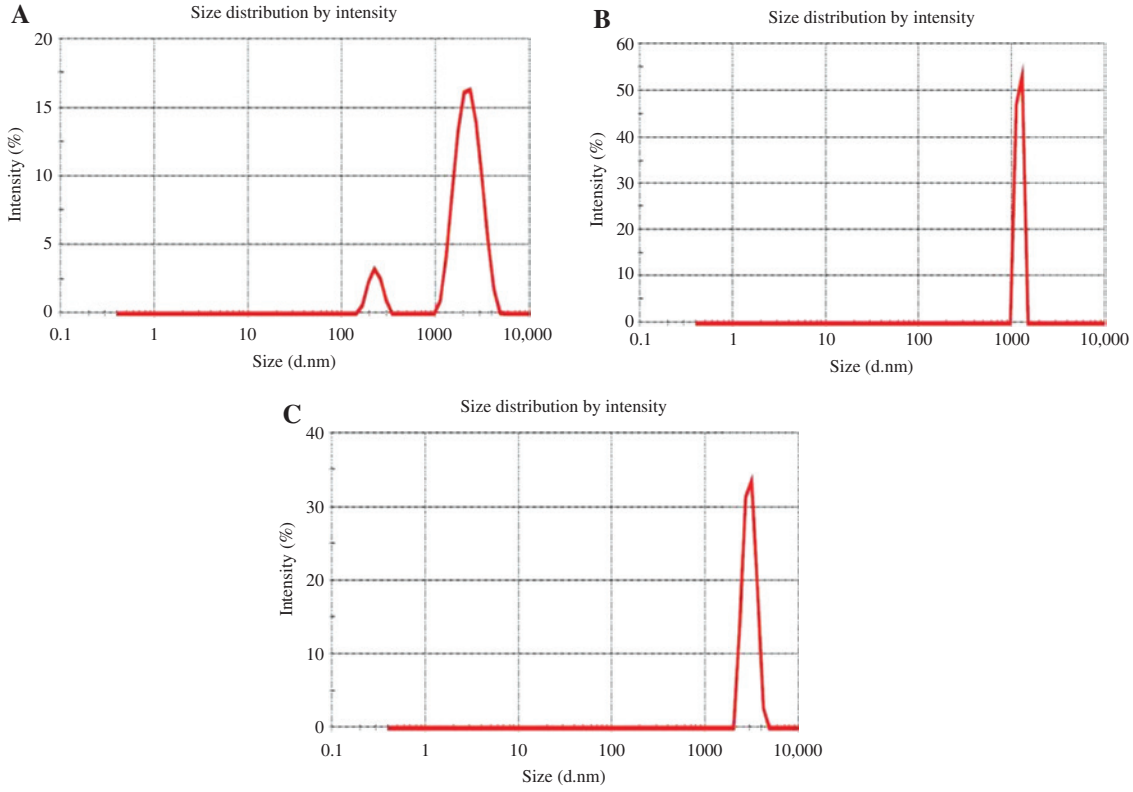

Figure 10: Size distributions of particles for A380 alloy/TiB_2 composites fabricated at 30 min AT and HTs of (A) 20 min, (B) 30 min, and (C) 40 min.

Table 3: Average particle sizes with respect to different HTs and ATs.

Average particle size (nm)			
AT (min)	HT (min)		
	20	30	40
10	1876	1639	1121
20	2187	782	473.4
30	2078	1199	2972

of the specimen is the most likely reason for this anomaly. Interestingly, the Al alloy displayed negligible hardness variation while all composites showed varying degrees of hardness variation. The former is an indication of the quality of the Al used, whereas the latter is a reflection of the non-uniformity of particle distribution. Figure 11B and C show the hardness distributions obtained for 20 min and 30 min AT, respectively, with different HT conditions. The hardness values in these conditions showed higher hardness than those in the Al alloy, although some variations in the values can also be observed.

Table 4 presents the average values of the hardness presented in Figure 11. The values within parenthesis are the deviations of hardness values from the average, which also represent the hardness variations. The highest hardness values were produced by composites with 20 min AT and 20 or 30 min HT. One of them also showed the smallest deviation from the mean. This result is not surprising as the microstructures of these composites (Figure 3A and B) displayed the least particle agglomeration. Meanwhile, the composite produced with 10 min AT and 20 min HT showed the largest hardness variation. This result was also expected because the clustering index of this composite (Figure 5) was the highest, indicating significant particle agglomeration. Hardness variations in all the other composites were very similar, consistent with the clustering indices of those composites.

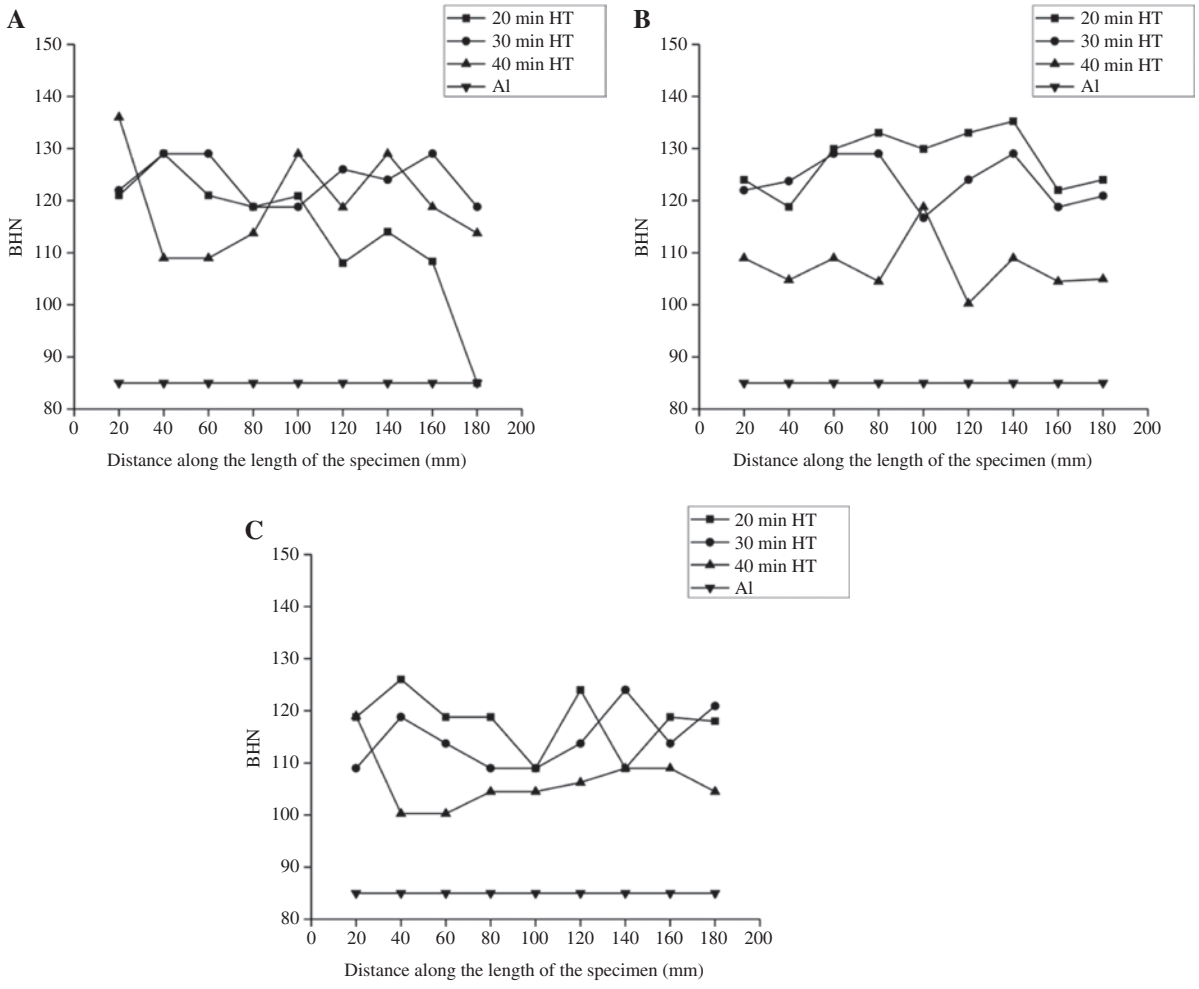

Figure 11: Influence of HT on hardness of Al/TiB_2 with constant AT of (A) 10 min, (B) 20 min, and (C) 30 min.

Table 4: Average hardness variation with respect to HT and AT.

Average values of hardness and standard deviation (±)			
AT (min)	HT (min)		
	20	30	40
10	114 (±12.8)	123 (±4.6)	119 (±9.6)
20	128 (±5.7)	125 (±4.5)	107 (±5.2)
30	118 (±5.7)	115 (±5.5)	106 (±5.6)

The hardness variation is due to the non-uniform distribution, which includes the absence of, or agglomeration of, TiB_2 particles. For instance, when the hardness measurement was performed at a location where there was no TiB_2 particle in the vicinity, the corresponding hardness value was lower than the average value. Similarly, hardness measurement performed at a location containing a cluster of TiB_2 particles registered values that were higher than the average values. Therefore, the degree of hardness variation is an indirect measure of the uniformity of particle distribution within the matrix. At a low AT of 10 min, the *in situ* particles became large in size due to the instantaneous reaction between the precursors. Hence, the particle settling rate was also high and led to agglomeration, as evidenced by the resulting microstructure (Figure 2A). As a result, the particles could not be dispersed evenly. However, the salts were added slowly at higher ATs of 20 and 30 min. As a result, the completion of the reaction between salts and particle formation took a long time. Consequently, smaller-sized particles were formed, which could be dispersed evenly. However, in some cases, the dispersion of particles was poor even at higher AT, which was due to higher HT. At prolonged HT, i.e. 40 min, the hardness value showed considerable variation. This was due to the formation of large particles and the resulting agglomeration. Lakhsmi et al. [23] reported a similar trend of increasing size of TiB_2 particle at higher HT.

From the above observation, at a constant AT of 10 min, the hardness increased to 7.9% and 4.9% when HTs were increased to 30 and 40 min, respectively, compared with the hardness of the composite processed at 20 min HT. At a constant AT of 20 min, the hardness decreased to 2.3% and 16.4% when HTs were increased to 30 and 40 min, respectively, compared with the 20 min HT. Further increasing the AT to 30 min, the hardness decreased to 2.5% and 10.2% when HTs were increased to 30 and 40 min, respectively, compared with 20 min HT.

Similarly, at constant HT of 20 min, the hardness increased to 12.28% and 3.5% when ATs were increased to 20 and 30 min, respectively, compared with the hardness of the composite processed at 10 min AT. However, at a constant HT of 30 min, the hardness increased to 1.6% and decreased to 6.5% when ATs were increased to 20 and 30 min, respectively, compared with the AT of 10 min. At HT of 40 min, the hardness decreased to 10.08% and 10.9% when ATs were increased to 20 and 30 min, respectively, compared with the AT of 10 min. The hardness measurements indicated that the composite processed at 20 min AT with 20 and 30 min HT conditions showed improved hardness value.

3.5 Tensile strength

Figure 12A and B show the variations in the yield stress (YS) and ultimate tensile strength (UTS) of Al/TiB_2 composites

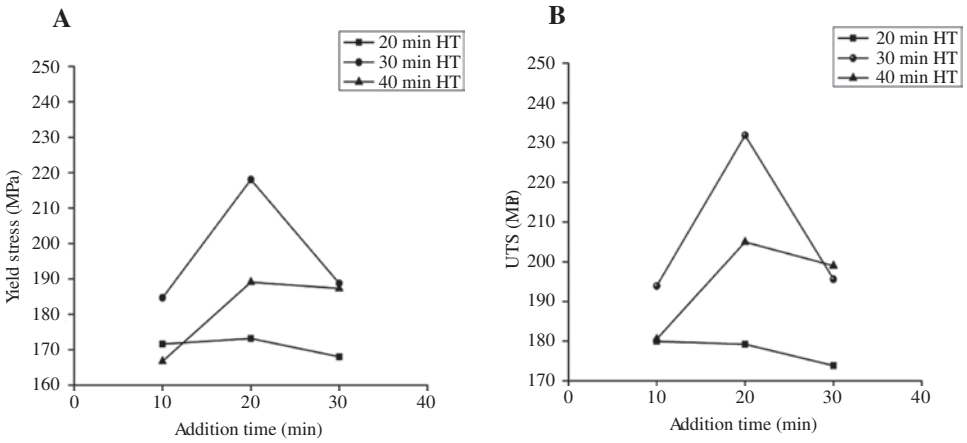

Figure 12: (A) Variations of yield stress (YS) with respect to constant AT (B) Variation of ultimate tensile strength (UTS) with respect to constant AT.

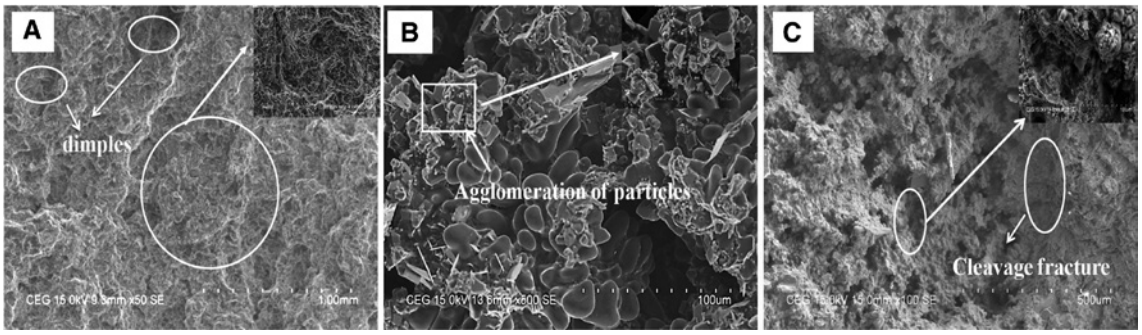

Figure 13: SEM images of fracture surfaces of the (A) Al alloy, (B) Composite under 10 min AT 20 and min HT, and (C) Composite under 20 min AT and 30 min HT.

with respect to HT and AT, respectively. The YS and UTS values of the Al matrix were 149.29 and 161.02 MPa, respectively. All composites processed using different combinations of ATs and HTs showed higher YS and UTS than the matrix material. In general, the strength increased when the AT was increased from 10 min to 20 min. One exception was the composite produced with 20 min AT and 20 min HT, which showed a slight decrease in UTS when the AT was increased from 10 min to 20 min. A further increase in AT resulted in decreased UTS for all composites. The HT also had a significant influence on the UTS. The strength increased when the HT was increased from 20 min to 30 min, but decreased with further increase in HT to 40 min. Particle agglomeration in the microstructure at higher HT was also seen (Figure 4C). The composite produced with 20 min AT and 30 min HT showed the largest UTS. This composite showed the least particle agglomeration (Figure 3B) and the second smallest particle size (Table 4). The small size of the particles and their uniform distribution contributed to the highest improvement in strength. In other cases, only a modest improvement in strength was observed because of large particle size and agglomeration.

From these results, we observed that the highest tensile strength was achieved in the Al/TiB_2 composite processed at 20 min AT with 30 min HT as a result of the uniform particle distribution of finer particles.

3.6 Fractography

Figure 13 shows the fracture surface of Al alloy and Al/TiB_2 composites. As can be seen, the dimples and tearing edges appeared on Al matrix material by coalescence of voids. This indicated the large plastic deformation of Al alloy (Figure 1A). The fracture surface of the composite sample processed with 10 min AT and 20 min HT is presented in Figure 13B as an example for the worst condition. The fracture surface showed particle agglomerations in the fractured surface. Therefore, the specimen processed at this condition failed at low strength and low strain. Meanwhile, the fracture surface of the composite prepared with 20 min AT 30 min HT condition showed (Figure 13C fair distribution of particles in the fracture surface. We also observed that the dimple formation was much lower in this case. Hence, the sample failed just like a brittle specimen.

4 Conclusions

Al composites containing 5wt.%TiB_2 were synthesized through chemical reaction between halide and salts in the presence Al melt. The TiB_2 formations were confirmed from the XRD results. Microstructure examination showed a good degree of uniform distribution particle obtained at 30 min HT and 20 min AT compared with other conditions.

The *in situ* reactions produced TiB_2 particles with a hexagonal shape. Coarse particles were formed when short AT of 10 min and HT of 20 min were used for processing, whereas fine particles were formed when 20 min AT with 40 min HT were used. Regardless of the HTs and ATs, the composites produced always displayed higher hardness than those of the Al alloy. In addition, composites produced with the AT of 20 min and HT of 20 or 30 min displayed the least hardness variation. The increase in the average hardness of the composite was 51% greater than that of the Al parent material.

The YS and UTS of the Al/TiB_2 composite were always higher than those of the Al alloy for all processing conditions. The highest YS and UTS values were obtained for the composite produced under 20 min AT and 30 min HT conditions. The increase in the UTS of the composite is 44% greater than that of the Al parent material.

Acknowledgments: One of the authors, Mr. A.S. Vivekananda, would like to thank the Anna University Chennai for the award of an Anna Centenary Research Fellowship for carrying out the research work.

References

[1] Zhao M, Wu G, Jiang L, Dou Z. *Compos. Part A Appl. Sci. Manuf.* 2006, 37, 1916–1921.
[2] Ramesh CS, Ahamed A. *Wear* 2011, 271, 1928–1939.
[3] Kuruvilla AK, Prasad KS, Bhanuprasad VV, Mahajan YR. *Scr. Metall. Mater*. 1990, 24, 873–878.
[4] Balasivanandha Prabu S, Karunamoorthy L, Kathiresan S, Mohan B. *J. Mater. Process. Technol.* 2006, 171, 268–273.
[5] Su B, Yan HG, Chen G, Shi JL, Chen JH, Zeng PL. *Mater. Sci. Eng. A* 2010, 527, 6660–6665.
[6] Sozhamannan GG, Balasivanandha Prabu S. *Mater. Charact.* 2009, 60, 986–990.
[7] Sadeghian Z, Enayati MH, Beiss P. *J. Mater. Sci.* 2009, 44, 2566–2572.
[8] Feng CF, Froyen L. *J. Mater. Sci.* 2000, 35, 837–850.
[9] Guo MX, Shen K, Wang MP. *Mater. Chem. Phys.* 2012, 131, 589–599.
[10] Khatri S, Koczak M. *Mater. Sci. Eng. A* 1993, 162, 153–162.
[11] Dhokey NB, Gule S, Rane K, Ranade RS. *Adv. Mater. Lett.* 2011, 2, 210–216.
[12] Xue J, Wang J, Han Y, Li P, Sun B. *J. Alloys Compd.* 2011, 509, 1573–1578.
[13] Watson IG, Forster MF, Lee PD, Dashwood RJ, Hamilton RW, Chirazi A. *Compos. Part A Appl. Sci. Manuf.* 2005, 36, 1177–1187.
[14] Chen ZY, Chen YY, Shu Q, An GY. *J. Mater. Sci.* 2000, 35, 5605–5608.
[15] Mallikarjuna C, Shashidhara SM, Mallik US, Parashivamurthy KI. *Mater. Des.* 2011, 32, 3554–3559.
[16] Emamy M, Mahta M, Rasizadeh J. *Compos. Sci. Technol.* 2006, 66, 1063–1066.
[17] Murty BS, Kori SA, Venkateswarlu K, Bhat RR, Chakraborty M. *J. Mater. Process. Technol.* 1999, 89–90, 152–158.
[18] Liu Z, Rakita M, Xu W, Wang X, Han Q. *Chem. Eng. J.* 2015, 263, 317–324.
[19] Lu L, Lai MO, Chen FL. *Acta Mater.* 1997, 45, 4297–4309.
[20] Gao Q, Wu S, Lü S, Duan X, An P. *Mater. Des.* 2016, 94, 79–86.
[21] Chen Z, Wang T, Zheng Y, Zhao Y, Kang H, Gao L. Mater. *Sci. Eng. A* 2014, 605, 301–309.
[22] Changizi A, Kalkanli A, Sevinc N. *J. Alloys Compd.* 2011, 509, 237–240.
[23] Lakshmi S, Lu L, Gupta M. *J. Mater. Process. Technol.* 1998, 73, 160–166.